Acta Oceanol. Sin., 2019, Vol. 38, No. 4, P. 106–115
https://doi.org/10.1007/s13131-019-1416-4
http://www.hyxb.org.cn
E-mail: hyxbe@263.net

Trends of sea surface temperature and sea surface temperature fronts in the South China Sea during 2003–2017

Yi Yu[1], Hao-Ran Zhang[1, 3], Jiangbo Jin[4], Yuntao Wang[1, 2*]

[1] State Key Laboratory of Satellite Ocean Environment Dynamics, Second Institute of Oceanography, Ministry of Natural Resources, Hangzhou 310012, China

[2] State Key Laboratory of Numerical Modeling for Atmospheric Sciences and Geophysical Fluid Dynamics, Institute of Atmospheric Physics, Chinese Academy of Sciences, Beijing 100029, China

[3] College of Oceanography, Hohai University, Nanjing 210098, China

[4] International Center for Climate and Environment Sciences, Institute of Atmospheric Physics, Chinese Academy of Sciences, Beijing 100029, China

Received 26 June 2018; accepted 20 August 2018

Abstract

The trends of the sea surface temperature (SST) and SST fronts in the South China Sea (SCS) are analyzed during 2003–2017 using high-resolution satellite data. The linear trend of the basin averaged SST is 0.31°C per decade, with the strongest warming identified in southeastern Vietnam. Although the rate of warming is comparable in summer and winter for the entire basin, the corresponding spatial patterns of the linear trend are substantially different between them. The SST trend to the west of the Luzon Strait is characterized by rapid warming in summer, exceeding approximately 0.6°C per decade, but the trend is insignificant in winter. The strongest warming trend occurs in the southeast of Vietnam in winter, with much less pronounced warming in summer. A positive trend of SST fronts is identified for the coast of China and is associated with increasing wind stress. The increasing trend of SST fronts is also found in the east of Vietnam. Large-scale circulation, such as El Niño, can influence the trends of the SST and SST fronts. A significant correlation is found between the SST anomaly and Niño3.4 index, and the ENSO signal leads by eight months. The basin averaged SST linear trends increase after the El Niño event (2009–2010), which is, at least, due to the rapid warming rate causing by the enhanced northeasterly wind. Peaks of positive anomalous SST and negatively anomalous SST fronts are found to co-occur with the strong El Niño events.

Key words: South China Sea, sea surface temperature, sea surface temperature fronts, warming trend, wind stress

Citation: Yu Yi, Zhang Hao-Ran, Jin Jiangbo, Wang Yuntao. 2019. Trends of sea surface temperature and sea surface temperature fronts in the South China Sea during 2003–2017. Acta Oceanologica Sinica, 38(4): 106–115, doi: 10.1007/s13131-019-1416-4

1 Introduction

With increasing atmospheric CO_2 and other greenhouse gas concentrations, the rate of global warming has increased significantly over the last 100 years (Levitus et al., 2005). Trenberth et al. (2007) found that the overall linear trend of global warming from 1906 to 2005 is approximately (0.07±0.02)°C per decade, which almost doubled ((0.13±0.03)°C per decade) during 1956–2005. Recent studies noted that the warming rate of global mean surface temperature decreased from 1997–2013 at a rate of approximately (0.07±0.08)°C per decade (Fyfe et al., 2013; Schmidt et al., 2014). The slowdown in the warming rate has been referred to as the global warming "hiatus" (Knight et al., 2009; Meehl et al., 2011). However, the global mean surface temperature has increased since 2014 (Blunden and Arndt, 2015, 2016, 2017). The global temperature reached a historical high in 2016 that was set in the mid-to-late 1800s (Blunden et al., 2017). And 2017 was the warmest year for the global ocean (Cheng and Zhu, 2018).

Although the increase in the global mean surface temperature in recent decades has been substantially prominent, the changing rates at different regions varied widely (Trenberth et al., 2007). On the other hand, some areas were characterized by a cooling trend in the same period. For example, the coastal stations in central Chile have a linear trend of –0.2°C per decade (Falvey and Garreaud, 2009). The northeastern Gulf of Mexico cooled for over three decades, but a warming trend was predominant in the western Gulf of Mexico and the Caribbean during the same period (Lluch-Cota et al., 2013). Given the huge spatial differences in the warming trend, it is important to investigate the SST trend at regional level.

The South China Sea (SCS) is the largest semi-enclosed marginal sea in the West Pacific. It occupies a surface area of approximately 3.5×10^6 km^2 that has an average depth of over 2 000 m. The SCS is constituted of a deep basin with two continental shelves and connects to the East China Sea, Northwest Pacific Ocean and Indian Ocean through the Taiwan Strait, Luzon Strait and Strait of Malacca, respectively. The SCS is key to water and

Foundation item: The National Key Research and Development Program of China under contract No. 2016YFC1401601; the Scientific Research Fund of the Second Institute of Oceanography, MNR under contract No. JB1806; the National Natural Science Foundation of China under contract Nos 41806026, 41806041, 41706036 and 41730536; the Project of State Key Laboratory of Satellite Ocean Environment Dynamics, Second Institute of Oceanography, MNR under contract No. SOEDZZ1902.
*Corresponding author, E-mail: yuntao.wang@sio.org.cn

heat exchange between the Pacific Ocean and Indian Ocean (Gao et al., 2015), and it has an important influence on the global climate. The East Asian monsoon plays an important role in determining the climate system of the SCS (Wyrtki, 1961; Liu and Xie, 1999; Su, 2004). The wind of the SCS is characterized by a southwest monsoon in summer, which reverses to the northeast in winter. The circulations in the upper SCS are consequently different under the influence of alternating monsoon systems (Xue et al., 2004; Liu et al., 2008).

Many investigations reported the trends of SST in the SCS over the past decades (Fang et al., 2006; Cai et al., 2009; Liu and Zhang, 2013; Wang et al., 2016). Studies showed the SST of SCS increased significantly in the past several decades (Liu and Zhang, 2013) and that the corresponding the rate of SST increase has been significantly higher than global warming rates (Fang et al., 2006). The patterns of the SST trend changed from increasing to decreasing before and after 2001 (Cheng and Qi, 2007; Wang et al., 2016). The warming trends in summer and winter were substantially different (Park and Choi, 2016), with a more prominent rate of increase in winter (Zhang et al., 2010).

Previous studies investigated the long-term trends of SST in the SCS, but most of them did not resolve the trends at different spatial location because of coarse resolutions. For example, the SST data used by Liu and Zhang (2013) and Wang et al. (2016) were from the Hadley Centre Sea Ice and SST model (HadISST, Rayner et al., 2003), with a spatial resolution of 1°×1°. The horizontal resolution of the data used by Yang and Wu (2012), obtained from the Simple Ocean Data Assimilation (SODA, Carton et al., 2005), had a resolution of 0.5°×0.5°. The low resolution resulted in difficulties in investigating the SST trends in the coastal regions. A detailed description with high spatial resolution for recent years is thus important for understanding the rate of SST changing in SCS, but such a description is not yet available.

The spatially non-uniformed SST and SST trend can induce an SST gradient, which is usually treated as an index of oceanic fronts (Shi et al., 2015). The oceanic fronts play an important part in the shelf marine system, such as the regional ecosystem, fisheries and the regional climate (Barth et al., 2007; Wang et al., 2016). A high-resolution SST product is required to resolve the SST gradient. The SST and SST fronts in the SCS are determined by different factors, e.g., wind stress, large scale circulation. Fang et al. (2006) found that the strong warming events in the SCS co-occurred with the El Niño events. The anomalous winds were associated with the shift in the SST trends in the SCS (Wang et al., 2016). Jing et al. (2016) revealed that the wind forcing largely impacted the seasonal frontal activities in the northern SCS.

With the limitation of coarse data resolution, the trend of SST in the coastal regions is difficult to investigate. In addition, the years from 2014 to 2017 are recorded as the warmest period since the 1800s, but the corresponding SST trend in the SCS has not been fully investigated. In the other hand, previous studies focused on the seasonal SST fronts, while the trends of SST fronts were not yet available. Therefore, in this study, a dataset with a 4-km spatial resolution is used to investigate the trends of the SST and SST fronts. We will also study their associations with El Niño events and variability of wind stresses. The remainder of the paper is organized as follows. Section 2 describes the datasets that we use in this study. The trends of SST, SST gradient and the impact of winds on them in the SCS are presented in Section 3. Section 4 contains the discussion and concluding remarks.

2 Data and methods

Satellite-derived sea surface temperature data from the moderate resolution imaging spectroradiometer (MODIS) was utilized to assess the trends of SST and the SST gradient over the SCS. The satellite data used to generate SST observations were retrieved from the US National Aeronautics and Space Administration, Ocean Biology Processing Group (NASA OBPG, Moradi and Kabiri, 2015). The observations used in this study were the standard level-4 data with a spatial resolution of 0.04°×0.04° (Esaias et al., 1998), which has been available since 2002. The period of SST used in this paper was from October 2002 to September 2017, a range of 15 years.

The sea winds data used in the present study are ERA-Interim reanalysis products. It is the latest global atmospheric reanalysis developed by the European Centre for Medium-Range Weather Forecasts (ECMWF, Dee et al., 2011). A four-dimensional variational (4D-VAR) data assimilation process was used in the ERA-Interim reanalysis to incorporate the observations by using a more dynamic method (Bracegirdle, 2013). The spatial resolution was approximately 0.25°×0.25°. Data from October 2002 to September 2017 were used in the current study, consistent with the time period of the SST data, and the ERA-Interim 10-m-high wind data were available from 1979 to present. The wind stress was calculated by the bulk formula, following Smith (1988). A more detailed description of the ERA-Interim reanalysis products can be found in Dee et al. (2011).

The SST data was smoothed with a 365-d running mean to eliminate the seasonal variability. The SST anomaly (SSTA) was subsequently calculated by removing the overall average. Thomson and Emery (2014) argued that the method could effectively remove signals with frequencies higher than one cycle per year. The 365-d running mean filters were applied for each grid point to remove the seasonal variability over the SCS. The linear trends of SST, or SST gradient magnitude, were then calculated through the method of least squares.

3 Results

3.1 *Trends of the South China Sea SST*

The spatial distribution of the linear trend of the SST during 2003–2017 reveals a significantly increasing trend in most of the SCS (Fig. 1). The only exceptions are some coastal areas, e.g., the Beibu Gulf, the Northern Taiwan Channel, and the east of Vietnam, which are associated with a large SST gradient (Xie et al., 2003; Jing et al., 2016). The trend of the basin-averaged SST in the SCS is approximately 0.31°C per decade during 2003–2017. Fang et al. (2006) indicated rates of 0.26°C per decade and 0.5°C per decade in the periods of 1982–2004 and 1993–2003, respectively. The basin-averaged warming trend calculated here is between these two studies, indicating a rapid warming tendency during 1993–2003 and a slowly increasing during 1982–1993 and during 2003–2017. The fastest warming trend is identified in the south of Vietnam (0.56°C per decade), almost double the rate of the basin-averaged trend. Another significantly large warming signal is found to the west of Luzon Island.

As mentioned above, the western Luzon (17°–21°N, 114°–118°E) and southern Vietnam (8°–12°N, 106°–110°E) are identified to have the greatest warming trends (Fig. 1). The time series of SSTA averaged over the two regions, together with that of the entire basin of the SCS, are calculated (Fig. 2). The basin-averaged SST has a warming trend of 0.31°C per decade, somewhat lower than that in the western Luzon (0.35°C per decade) and much smaller than southern Vietnam (Table 1). For the three areas, we observed that the time series of SSTA are almost identical between 2003 and 2007 and corresponding correlation coefficients between each two of them are significant. The time

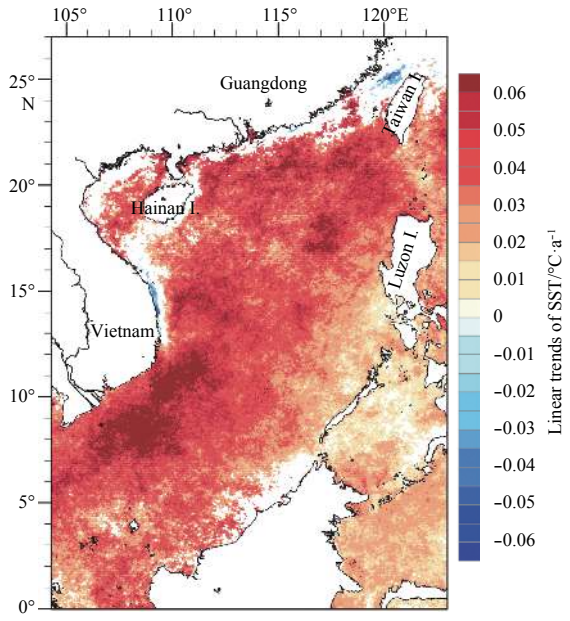

Fig. 1. Linear trends of SST during 2003–2017. The non-significant trends at the 95% confidence level are not plotted.

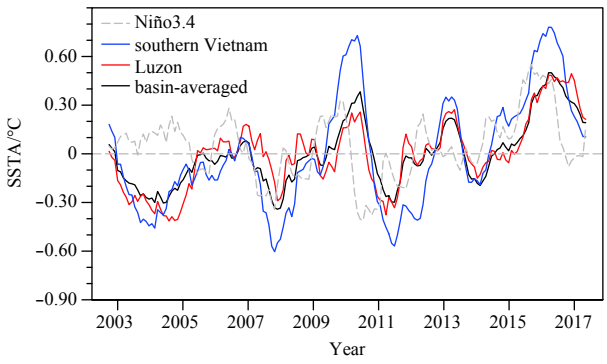

Fig. 2. Time series of the SST anomalies for basin-averaged (black), western Luzon (red) and southern Vietnam (blue), overlaid with the normalized Niño3.4 index (gray). The western Luzon and southern Vietnam are defined as (17°–21°N, 114°–118°E) and (8°–12°N, 106°–110°E), respectively.

Table 1. Linear trends of the SST, correlation coefficients and time lags for the maximum correlations between SSTA and the Niño3.4 index in the SCS, western Luzon and southern Vietnam during 2003–2017

	SCS	Western Luzon	Southern Vietnam
Trend/°C per decade	0.31	0.35	0.44
Simultaneous correlation coefficients	0.28	0.19	0.39
Time lags for the maximum correlations/months	8	8	7
The maximum correlation coefficients	0.69	0.59	0.76

series among them are still highly correlated after 2007, however, the SSTA in the southern Vietnam had much higher fluctuations than the others.

Thompson et al. (2017) found that the linear trend over the SCS clearly shifted in the pre- and post-years of El Niño events. In our study, the SCS SST also presents a distinctive pattern in pre- and post-years of 2009–2010 when an El Niño event occurred. The basin-averaged SST linear trend is six times larger during 2011–2017 than it is during 2003–2008 (Table 2). We further compared the spatial patterns of the SST linear trends during 2003–2008 and 2011–2017 in Fig. 3. The results clearly indicate that the patterns of warming in the two periods are significantly different. As expected, prominent SST warming in the period of 2011–2017 can be found for the majority of the SCS. The only exceptions are a few regions, e.g., the northern Luzon Island and northwestern Beibu Gulf, which are characterized by a weak cooling process. In contrast to the general warming pattern during 2011–2017, a strong cooling trend during 2003–2008 occurs in a large portion of the basin, especially in the coastal area of China. It is interesting to notice that the simultaneous warming trend in the Luzon Strait (18°–22°N, 119°–121°E) is surprisingly large, reaching 1.15°C per decade (Table 2). Note that the linear trend in the southeastern Vietnam (6°–12°N, 108°–114°E) during 2003–2008 is negative (–0.23°C per decade) and becomes positive during 2011–2017 (Table 2).

Table 2. Linear trends of the SST (°C per decade) in the SCS, Luzon Strait and southeastern Vietnam during 2003–2008 and 2011–2017

Period	SCS	Luzon Strait	Southeastern Vietnam
2003–2008	0.13	1.15	–0.23
2011–2017	0.94	0.23	0.89

The relationship between the SST in the SCS and the El Niño events is further investigated. The time series of the SSTA and the Niño3.4 index is highly correlated (Fig. 2). The correlation coefficients are calculated between Niño3.4 index and the SCS, western Luzon and southern Vietnam (Table 1). The positive peaks of SSTA in the SCS co-occur with the El Niño events, e.g., 2009–2010 and 2015–2016. Strong warming events in the SCS occurring during the El Niño have also been reported by Wang et al. (2002), Fang et al. (2006) and Thompson et al. (2017). The correlation coefficient between SSTA and Niño3.4 index is 0.28 for the overall period from 2003 to 2017, but it increases to 0.34 for 2008–2017. We also calculated the time lags between the SSTA and Niño3.4 index to identify when their correlations reach the maximum (Table 1). The SSTA in the SCS has the maximum correlation with Niño3.4 at an eight-month lag, with a correlation coefficient of 0.69. The results are consistent with Fang et al. (2006), but the maximum correlation coefficient is larger in our study.

The climatological mean (15 year averaged) SST in summer (June, July and August) and in winter (December, January and February) are shown in Figs 4a and b, respectively. The basin-averaged SST in summer (28.9°C) is approximately 3°C higher than that in winter (25.6°C). The spatial patterns of the climatological mean SST are very different between summer and winter. In summer, a jet with low SST can be observed in the southeast of Vietnam approximately 13°N. Xie et al. (2003) noted that the monsoon winds and anticyclonic circulation drive upwelling in this region. Thus, a cold core appears in the southeast of Vietnam. In winter, the anti-clockwise circulation driven by the northeast monsoon can transport cold water from the coast of China southward via the coast of Vietnam. Thus, low (high) SST is found in the northwest (southeast) of the SCS during winter (Fig. 4b).

In addition, we calculate the linear trend of SST in the summer (Fig. 4c) and winter (Fig. 4d). The basin-averaged SST has a

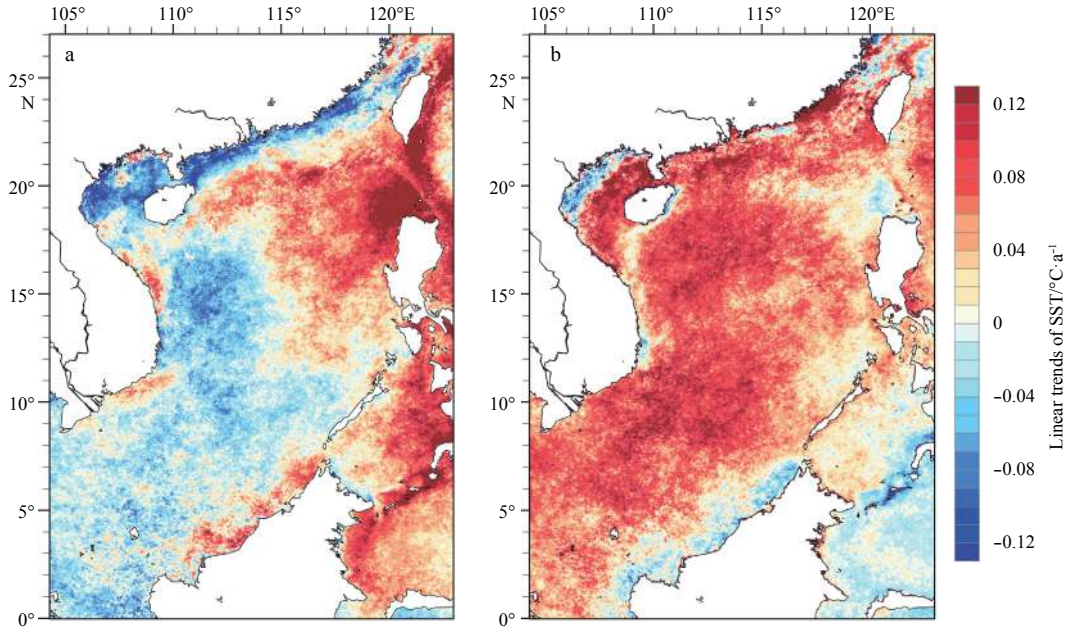

Fig. 3. Linear trends of SST in the SCS during 2003–2008 (a) and 2011–2017 (b).

warming trend of 0.42°C per decade and 0.39°C per decade in summer and winter, respectively. Yang and Wu (2012) reported the warming trend was 0.12°C per decade in summer and 0.15°C per decade in winter in the period of 1959–2008. The warming rate in our study is significantly higher than that found by Yang and Wu (2012). During summer, the largest warming trend is found to the west of the Luzon Strait, exceeding 0.6°C per decade. Another warming center is located in the middle basin of the SCS (approximately 14°N, 116°E). The SST trend in winter is characterized by a rapidly warming center in the middle of the SCS basin (approximately 15°N, 115°E) and southeast of Vietnam. The area with the rapid warming trend is larger in winter than it is in summer.

3.2 *Trends of the South China Sea SST fronts*

The SST front is a typical mesoscale oceanic dynamic and plays an important role in the air-sea interaction and biogeochemical processes in the coastal region (Belkin et al., 2009). The satellite observations of SST with a horizontal resolution of 0.04°×0.04° provide a robust approach to detect fronts in the SCS. The magnitude of the SST gradient can be used as the index to describe the strength of the SST fronts (Shi et al., 2015). Wang et al. (2015) found that the spatial patterns between the magnitude of the SST gradients and SST fronts were similar for different regions. Hence, the SST fronts are defined as regions with large-magnitude SST gradients in our study. The annual mean magnitude of SST gradient during 2003–2017 in the SCS is shown in Fig. 5a, which describes the spatial pattern for SST fronts. The SST fronts occur mainly in the regions where the SST gradient is greater than 0.01°C/km. The largest magnitude of the SST gradient occurs in the coast of China, with a value exceeding 0.04°C/km. Other regions with a large SST gradient magnitude include the coast of Vietnam, northwest of Luzon Island and Beibu Gulf. The spatial patterns of the linear trends of SST fronts (Fig. 5b) reveal prominent positive trends in the coast of China and the east of Vietnam. It is noted that these two areas have the largest SST gradient trends, but there exists in-significant warming (even cooling) trends in these two regions. In contrast, the Beibu Gulf and the northwest of Luzon Island are characterized by negative SST front trends.

A quantitative analysis is conducted to evaluate the linear trends of the SST fronts in SCS, particularly for the coast of China (22°–25°N, 111°–120°E) and the east of Vietnam (10°–16°N, 108°–111°E). The magnitude of the SST gradient in the coast of China reaches 0.024°C/km, which is approximately double the value in the east of Vietnam (0.013°C/km). However, the linear trends have similar values along the coast of China (0.11×10^{-3}°C/km per year) and the east of Vietnam (0.09×10^{-3}°C/km per year). The results illustrate that the SST fronts in the east of Vietnam increase more prominent than do those in the coast of China.

The time series of the region-averaged SST gradient anomaly in the coast of China (22°–25°N, 111°–120°E) and the east of Vietnam (10°–16°N, 108°–111°E) are shown in Fig. 6, overlaid with the normalized inverse Niño3.4 index during 2003–2017. The trough of the SST gradient anomaly generally occurs during El Niño events. However, the correlation coefficients between the Niño3.4 index and the SST gradient anomalies along the coast of China (–0.24) and east of Vietnam (0.11) are not significant, indicating that the influence of a large-scale global signal on the variability of SST fronts may be less pronounced.

The spatial patterns of the 15-year averaged magnitude of the SST gradient are prominently different in summer (Fig. 7a) and winter (Fig. 7b). The SST fronts in the coast of China occur all year round with a slight reduction in summer. In contrast, the SST fronts in the Beibu Gulf and northwest of Luzon Island occur in winter and disappear in summer. The seasonal variability of the SST fronts has been well explained by Shi et al. (2015). The southeast of Vietnam has a summer upwelling induced by strong wind curls (Xie et al., 2003), resulting in strong SST fronts to the southeast of Vietnam (Fig. 7a). The positive linear trends are found year-round along the coast of China, although the location of the largest positive linear trends changes distinctively in summer and winter. During the summer, the largest linear trends appear in the Taiwan Strait and move towards the coast of the Guangdong Province in winter. Interestingly, the SST fronts are

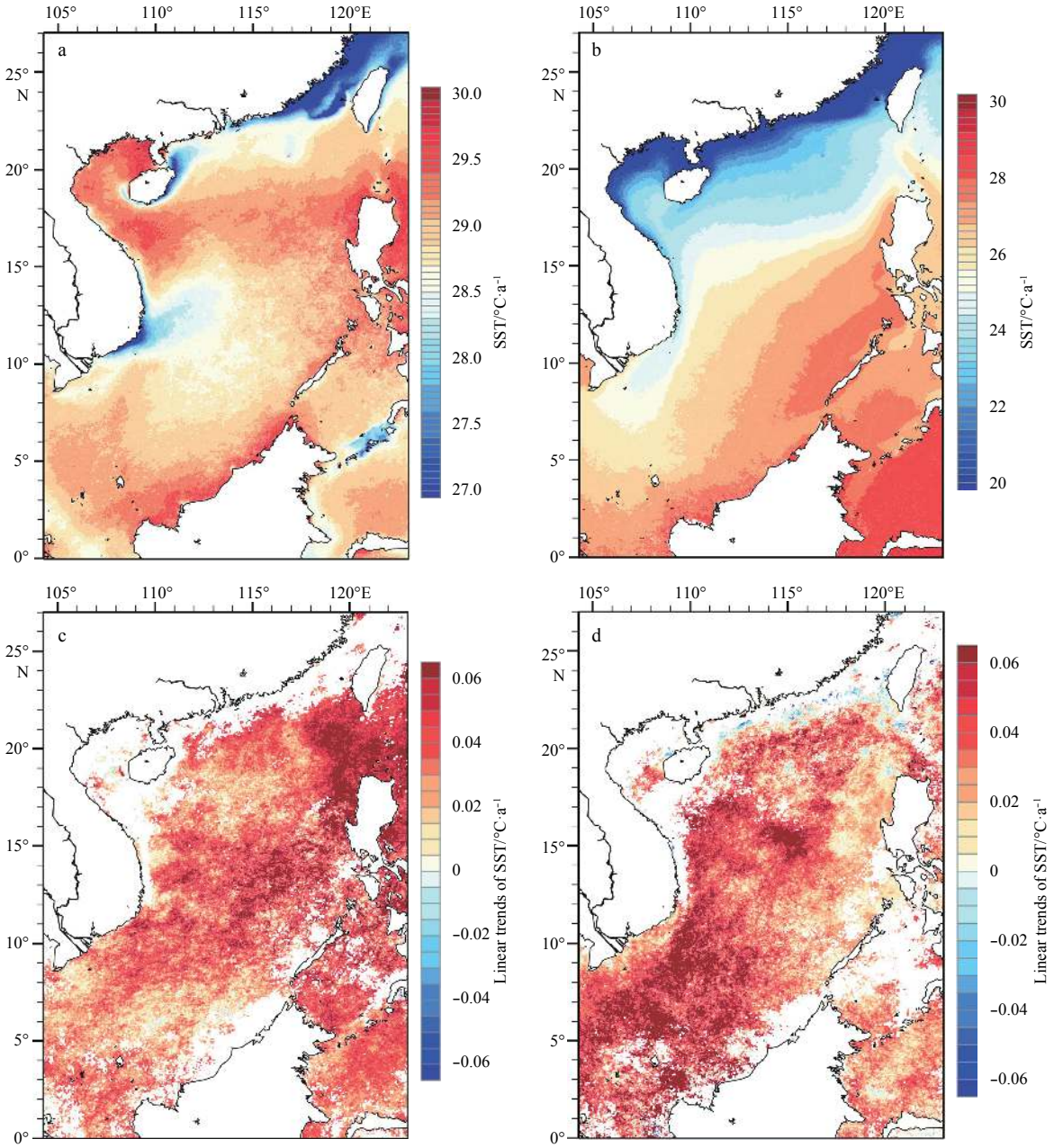

Fig. 4. Climatological mean SST (upper row), and linear trends of SST (lower row) in the SCS during 2003–2017 in the summer (left column) and in the winter (right column). The trends that are not significant at the 95% confidence level are not plotted.

stronger to the southeast of Vietnam than eastern Vietnam in summer (Fig. 7a), but the linear trends of the SST gradient magnitude are weaker for the southeast of Vietnam (Fig. 7c). It is noted that the southeast of Hainan Island is characterized by a significant positive linear trend in both summer and winter.

3.3 *Impact of the wind stress trend on the trends of the SST and SST fronts*

It is well known that the wind pattern of the SCS basin is dominated by the East Asian monsoon (Wyrtki, 1961; Fang et al., 2006). The southwesterly monsoon wind in summer and the northeasterly monsoon wind in winter can be seen in Figs 8a and b, respectively. Southwesterly winds can generate an anticyclonic circulation in summer, whereas a cyclonic circulation is driven by northeasterly wind in winter. From Figs 4, 7 and 8, we can see that the climatological mean SST and SST fronts are under the influence of the seasonal surface winds. Due to the southwesterly wind, summer upwelling is generated along the southeastern coast of Vietnam (Xie et al., 2003). This oceanic process results in a cold SST center (Fig. 4a) and SST fronts (Fig. 7a) in southeastern Vietnam. In winter, the coast of China shows prominent SST fronts (Fig. 7b), and the corresponding SST increases offshore from the coast (Fig. 4b). Figure 8b illustrates that the wind stress vectors get weaker over the lower SST, as compared to the warmer side of the front. This result reveals a positive correlation between SST and wind, consistent with the findings from Wang and Castelao (2016). The local impact of the SST fronts on surface wind has also been reported in earlier studies, such as Chelton and Xie (2011), and Shi et al. (2015).

The dominant patterns of the linear trend of wind stress in the

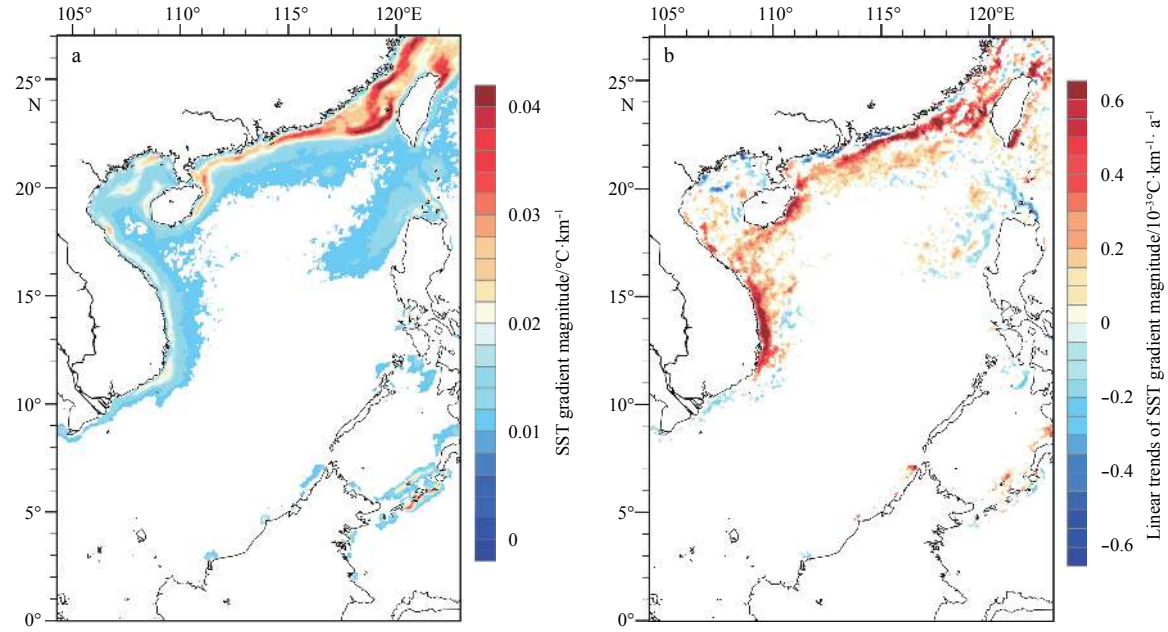

Fig. 5. Climatological annual mean SST gradient magnitude (a) and linear trends of SST gradient magnitude (b) in the SCS during 2003–2017. Regions with SST gradient magnitude <0.01°C/km are masked in both plots. In the right plot, the trends that are not significant at the 95% confidence level are not plotted.

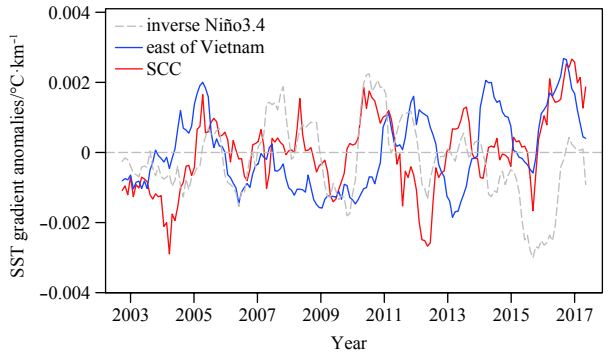

Fig. 6. Time series of the SST gradient anomalies for SCC (red, southeast coast of China) and east of Vietnam (blue), overlaid with the normalized inverse Niño3.4 index (gray).

SCS are very different between summer and winter (Figs 8c and d). Substantially stronger linear trends of wind stress are found in winter than in summer for most of the SCS basin, especially the northern part. Note that the linear trends of wind stress generate a cyclonic anomaly in both seasons near the Luzon Strait. As shown in Fig. 8c, there is a northeasterly wind stress anomaly off southeastern Vietnam, indicating that the southwesterly wind stress gets weakened in summer. The change of wind stress can reduce the summer upwelling and the strength of Southeast Vietnam Offshore Current. As a result, the cold core in southeastern Vietnam, which can be observed in Fig. 4a, becomes weaker and an increased warming trend in summer (Fig. 4c) is anticipated due to the reduced upwelling. Since the summer upwelling can induce strong SST fronts in this area (Fig. 7a), the SST fronts are expected to have a weak negative linear trend. However, the negative linear trend is not significant in southeastern Vietnam, even there exists a positive trend in eastern Vietnam (Fig. 7c). In winter, a weakened northeasterly wind stress can be found in the southwest of the SCS (0–6°N, 105–115°E), caused by the increasing southwesterly wind stress (Fig. 8d). The weakened northeasterly wind can reduce heat loss from the ocean (Park and Choi, 2016), so there is a significant warming in this area (Fig. 4d). The positive correlation identified in the coast of China between SST and wind stress is associated with the positive linear trends of the SST fronts (Fig. 7d). Consistently, the linear trends of wind stress in winter are high over the warm water and low over the cold water during 2003–2017.

As shown before, the linear trend of the basin-averaged SST is six times larger during 2011–2017 than it is during 2003–2008 (Table 2). The spatial patterns of SST warming can also be divided into two stages (Fig. 3). To explore the potential mechanisms for the different SSTA in the two periods, we present the linear trends of surface wind stress in the SCS during 2003–2008 and 2011–2017 in Fig. 9. The northerly wind stress anomaly and southerly wind stress anomaly can be observed clearly in Fig. 9 during 2003–2008 and 2011–2017, respectively. The opposite linear trend of SST in the east of Vietnam (Fig. 3) is accompanied by an opposite linear trend in the wind stress fields in the different periods. Fang et al. (2006) revealed that the annual mean surface wind is dominated by northeasterly winds. Thus, the northeasterly wind is strengthened during 2003–2008, and weakened during 2011–2017. The southerly wind anomaly in the east of Vietnam can induce a reduction of air advections, which will increase the cloud coverage (Wang et al., 2016), and decrease the heat loss to the air. With the influence of the wind stress anomaly, the east of Vietnam showed warming during 2011–2017, in contrast to the cooling process during 2003–2008. To the contrary, the Luzon Strait is characterized by a persistent warming signal, but the trend of wind stress is not conspicuous during 2003–2008. This may be caused by the transport in the Luzon Strait, which needs further investigation in future studies.

4 Discussion and concluding remarks

Based on high-resolution satellite SST observations, the trends of the SST and SST fronts in the SCS during 2003–2017 are

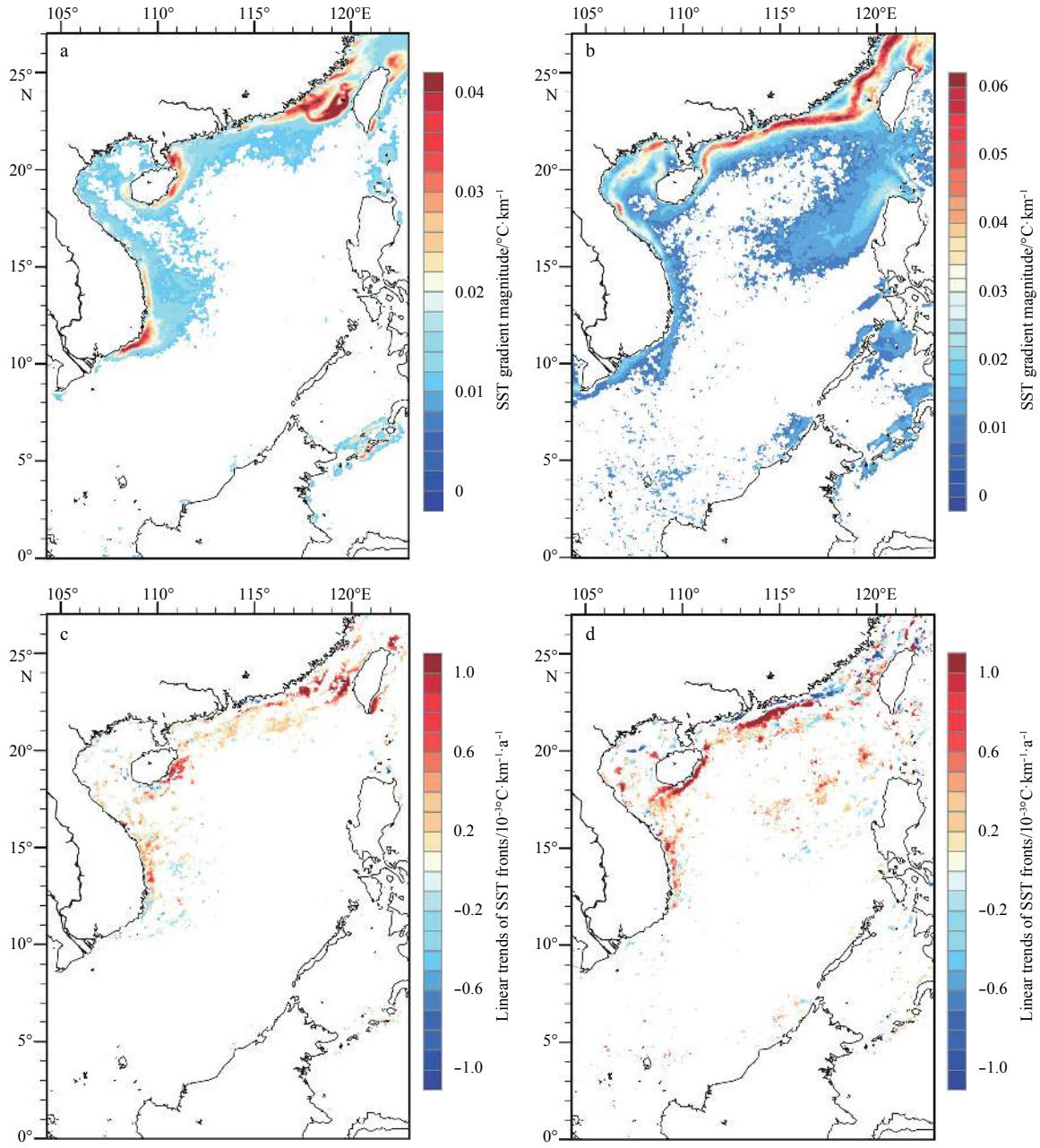

Fig. 7. Climatological mean SST gradient magnitude (upper row), and the linear trends of the SST fronts (lower row) in the SCS during 2003–2017 in summer (left column) and winter (right column). Regions with an SST gradient magnitude <0.01°C/km are masked in all plots. The trends that are not significant at the 95% confidence level are not plotted in the lower plots.

investigated in the present study. The basin-averaged warming trend is 0.31°C per decade during 2003–2017. And 2017 was the warmest year on record for the global ocean (Cheng and Zhu, 2018), however, it was not the warmest year in the SCS. Fang et al. (2006) showed that the linear trends of SST are 0.50°C per decade and 0.26°C per decade during 1993–2003 and 1982–2004, respectively. Thompson et al. (2017) calculated the warming trends in the SCS for 1982–2014 as 0.17°C per decade. This result indicates that the SST of SCS is increasing over the last decades, whereas the strength of warming rate exhibits great uncertainty. In our study, the time series is limited, with only 15 years. However, the difference in the warming rate is also found pre- and post-years of 2009–2010, when an El Niño event happened. The basin-averaged SST linear trend during 2011–2017 is six times larger than that during 2003–2008 (Table 2). The spatial patterns of the warming trend also exhibit distinctive patterns in different periods. A negative trend is identified for most of the SCS during 2003–2008, in contrast to the warming trend during 2011–2017, except the northwest of Luzon Island (Fig. 3). The difference in the warming trends may be induced by the change of wind stress (Fig. 9), specifically the northerly wind stress anomaly during 2003–2008 and southerly wind stress anomaly during 2011–2017. During 2011–2017, the northerly wind stress weakens, resulting in the reduction of heat loss to air (Park and Choi, 2016) and, thus, a warming trend in the basin, especially in the east of Vietnam.

Furthermore, we studied the linear trend of the SST and SST fronts in the SCS in both summer and winter. Although the

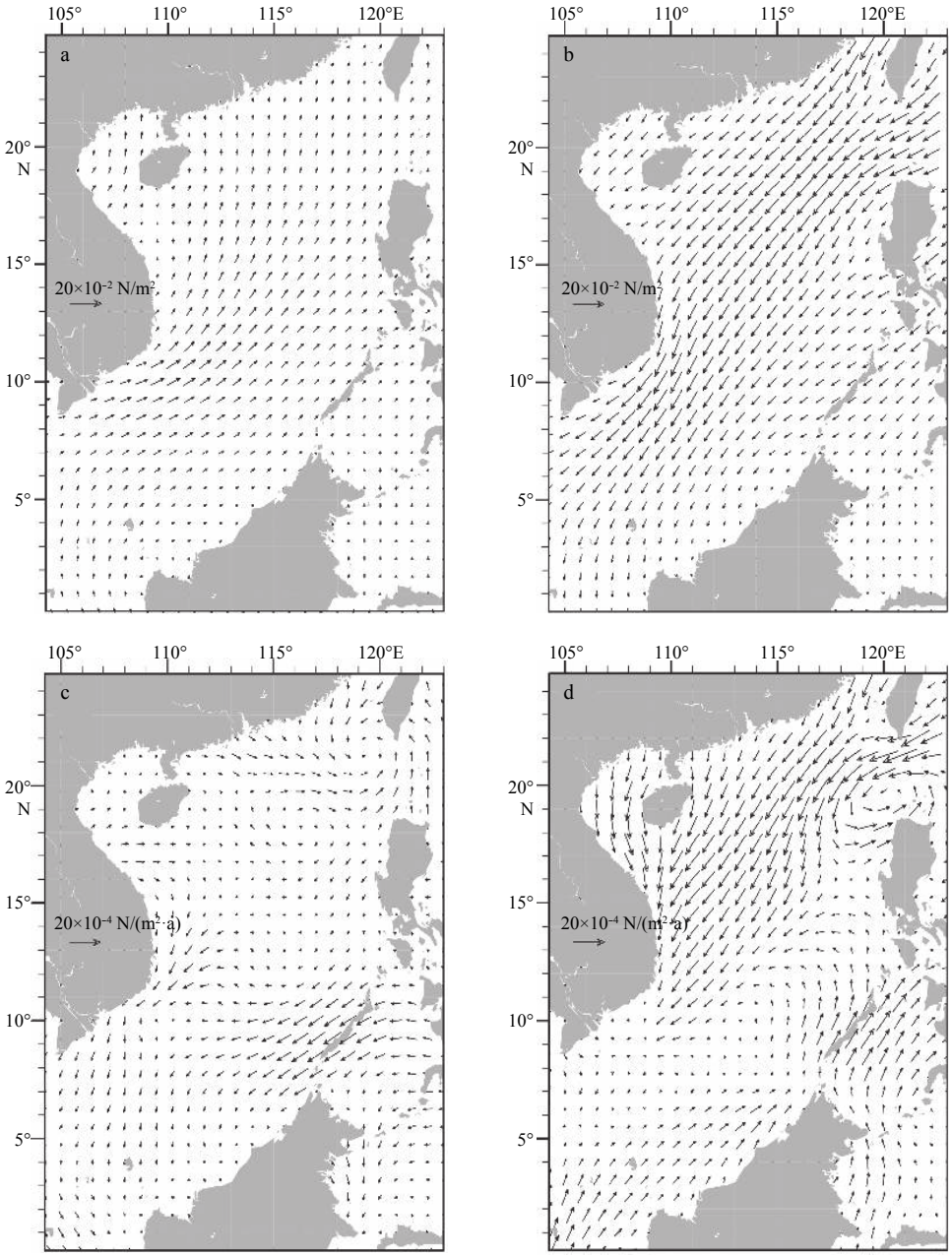

Fig. 8. Climatological mean surface wind stress (upper row), and linear trends of surface wind stress (lower row) in the SCS during 2003–2017 in summer (left column) and winter (right column).

warming trend of the basin-averaged SST was observed in both seasons, the spatial patterns of the linear trend were quite different. In summer, the most prominent warming rate is located in the west of the Luzon Strait, exceeding approximately 0.6°C per decade, while the strongest warming trend occurs to the southeast of Vietnam in winter. The most prominent trends of the SST fronts are found near the coast of China, which are characterized by an overall increasing trend. The southeastern coast of Vietnam has strong SST fronts due to the upwelling in summer, but the corresponding trend is negative. By analyzing the trends of wind stress, we verify that wind stress plays an important role in determining the trends of the SST and SST fronts. The northeasterly wind stress anomaly off southeastern Vietnam leads to a weakened southwesterly wind stress in summer. It will further reduce the summer upwelling and the Southeast Vietnam Offshore Current. Thus, the cold core becomes weaker and generates an increase warming trend in summer (Fig. 4c).

The correlation between the warming in the SCS and Niño3.4 index is also investigated in our study. First, the warming rate of the SCS accelerated in the years after the El Niño event (2009–2010). The shift of the warming rate in the SCS has also been reported in earlier studies, such as Wang et al. (2016) and Thompson et al. (2017). The response of SSTA to the Niño3.4 index is opposite that of SST gradient magnitude anomaly. The positive peaks of SSTA and negative peaks of SST gradient magnitude anomaly co-occur with the El Niño events, especially during strong events (2009–2010, 2015–2016). The SSTA in the SCS has the maximum correlation with Niño3.4 at an eight-month lag with Niño leading, consistent with Fang et al. (2006). These results confirm the great impact of large-scale circulation on SSTA at re-

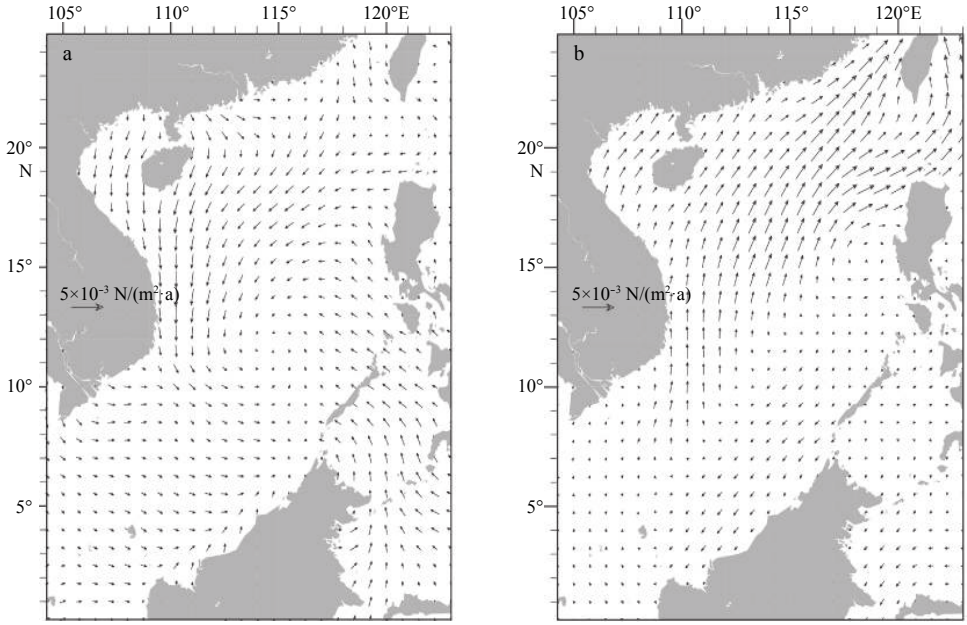

Fig. 9. Linear trends of surface wind stress in the SCS during 2003–2008 (a) and 2011–2017 (b).

gional scale.

The change of SST is generally associated with the variability of SST fronts. The trends of SST fronts had been studied in some of previous literature. In this study, we further found the SST gradient magnitude in the coast of China approximately doubled the value in the east of Vietnam. However, the linear trends of SST fronts had similar values in the coast of China and the east of Vietnam. The results illustrated that the SST fronts in the east of Vietnam increased more prominent than the coast of China. On the other hand, the two regions with prominent positive SST fronts trends were characterized by in-significant warming (even cooling) trends. We supposed that the stronger SST fronts activities have important impact on the SST warming in the coastal areas. We also investigated the correlation between the SSTA and SST fronts in the SCS and Niño3.4 index. The correlation between the SSTA in the SCS and Niño 3.4 index is larger than that SST fronts. The influence of large-scale global signal may be less pronounced on the variability of SST fronts, compared to the SSTA in SCS.

The potential mechanisms that can influence the trends of the SST and SST fronts are also explored by investigating the wind stress dynamics. However, the other driving forces for basin-scale changes in the SCS have been well discussed in several former studies and are thus not the major focus of our study. For example, Wang et al. (2016) revealed that the warming trends in the SCS are attributed to the surface heat flux. The SCS throughflow has a close relationship to the shift of the SST pattern in the SCS (Thompson et al., 2017). Further discussion regarding the post influence of the strong El Niño in 2016 would be fundamentally important to understanding the regional dynamics. The impact of the other factors (such as surface heat flux, eddy activities) on the trends of the SST fronts in the SCS will be investigated in future.

References

Barth J A, Menge B A, Lubchenco J, et al. 2007. Delayed upwelling alters nearshore coastal ocean ecosystems in the northern California current. Proceedings of the National Academy of Sciences of the United States of America, 104(10): 3719–3724, doi: 10.1073/pnas.0700462104

Belkin I M, Cornillon P C, Sherman K. 2009. Fronts in large marine ecosystems. Progress in Oceanography, 81(1-4): 223–236, doi: 10.1016/j.pocean.2009.04.015

Blunden J, Arndt D S. 2015. State of the climate in 2014. Bulletin of the American Meteorological Society, 96(7): ES1–ES32, doi: 10.1175/2015BAMSStateoftheClimate.1

Blunden J, Arndt D S. 2016. State of the climate in 2015. Bulletin of the American Meteorological Society, 97(8): Si–S275, doi: 10.1175/2016BAMSStateoftheClimate.1

Blunden J, Arndt D S. 2017. State of the climate in 2016. Bulletin of the American Meteorological Society, 98(8): Si–S280, doi: 10.1175/2017BAMSStateoftheClimate.1

Bracegirdle T J. 2013. Climatology and recent increase of westerly winds over the Amundsen Sea derived from six reanalyses. International Journal of Climatology, 33(4): 843–851, doi: 10.1002/joc.v33.4

Cai Rongshuo, Zhang Qilong, Qi Qinghua. 2009. Spatial temporal oscillation and long-term variation in sea surface temperature field of the South China Sea. Journal of Oceanography in Taiwan Strait (in Chinese), 28(4): 559–568

Carton J A, Giese B S, Grodsky S A. 2005. Sea level rise and the warming of the oceans in the Simple Ocean Data Assimilation (SODA) ocean reanalysis. Journal of Geophysical Research: Oceans, 110(C9): C09006

Chelton D B, Xie S P. 2011. Coupled ocean-atmosphere interaction at oceanic mesoscales. Oceanography, 23(4): 52–69

Cheng Lijing, Jiang Zhu. 2018. 2017 was the warmest year on record for the global ocean. Advances in Atmospheric Sciences, 35: 3261–3263

Cheng Xuhua, Qi Yiquan. 2007. Trends of sea level variations in the South China Sea from merged altimetry data. Global and Planetary Change, 57(3–4): 371–382, doi: 10.1016/j.gloplacha.2007.01.005

Dee D P, Uppala S M, Simmons A J, et al. 2011. The ERA-Interim reanalysis: Configuration and performance of the data assimilation system. Quarterly Journal of the Royal Meteorological Society, 137(656): 553–597, doi: 10.1002/qj.v137.656

Esaias W E, Abbott M R, Barton I, et al. 1998. An overview of MODIS capabilities for ocean science observations. IEEE Transactions on Geoscience and Remote Sensing, 36(4): 1250–1265, doi: 10.1109/36.701076

Falvey M, Garreaud R D. 2009. Regional cooling in a warming world:

Recent temperature trends in the southeast Pacific and along the west coast of subtropical South America (1979–2006). Journal of Geophysical Research: Atmospheres, 114(D4): D04102

Fang Guohong, Chen Haiying, Wei Zexun, et al. 2006. Trends and interannual variability of the South China Sea surface winds, surface height, and surface temperature in the recent decade. Journal of Geophysical Research: Oceans, 111(C11): C11S16

Fyfe J C, Gillett N P, Zwiers F W. 2013. Overestimated global warming over the past 20 years. Nature Climate Change, 3(9): 767–769, doi: 10.1038/nclimate1972

Gao Xiumin, Wei Zexun, Lv Xianqing, et al. 2015. Numerical study of tidal dynamics in the South China Sea with adjoint method. Ocean Modelling, 92: 101–114, doi: 10.1016/j.ocemod.2015.05.010

Jing Zhioyu, Qi Yiquan, Fox-Kemper B, et al. 2016. Seasonal thermal fronts on the northern South China Sea shelf: Satellite measurements and three repeated field surveys. Journal of Geophysical Research: Oceans, 121(3): 1914–1930, doi: 10.1002/2015JC011222

Knight J, Kennedy J J, Folland C, et al. 2009. Do global temperature trends over the last decade falsify climate predictions? In state of the climate in 2008. Bulletin of the American Meteorological Society, 90(8): 22–23

Levitus S, Antonov J, Boyer T. 2005. Warming of the world ocean, 1955-2003. Geophysical Research Letters, 32(2): L02604

Liu Qinyu, Kaneko A, Su Jilan. 2008. Recent progress in studies of the South China Sea circulation. Journal of Oceanography, 64(5): 753–762, doi: 10.1007/s10872-008-0063-8

Liu W T, Xie Xiaosu. 1999. Space based observations of the seasonal changes of South Asian monsoons and oceanic responses. Geophysical Research Letters, 26(10): 1473–1476, doi: 10.1029/1999GL900289

Liu Qinyu, Zhang Qi. 2013. Analysis on long-term change of sea surface temperature in the China Seas. Journal of Ocean University of China, 12(2): 295–300, doi: 10.1007/s11802-013-2172-2

Lluch-Cota S E, Tripp-Valdéz M, Lluch-Cota D B, et al. 2013. Recent trends in sea surface temperature off Mexico. Atmósfera, 26(4): 537–546, doi: 10.1016/S0187-6236(13)71094-4

Meehl G A, Arblaster J M, Fasullo J T, et al. 2011. Model-based evidence of deep-ocean heat uptake during surface-temperature hiatus periods. Nature Climate Change, 1(7): 360–364, doi: 10.1038/nclimate1229

Moradi M, Kabiri K. 2015. Spatio-temporal variability of SST and Chlorophyll-*a* from MODIS data in the Persian Gulf. Marine Pollution Bulletin, 98(1–2): 14–25, doi: 10.1016/j.marpolbul.2015.07.018

Park Y G, Choi A. 2016. Long-term changes of South China Sea surface temperatures in winter and summer. Continental Shelf Research, 143: 185–193

Rayner N A, Parker D E, Horton E B, et al. 2003. Global analyses of sea surface temperature, sea ice, and night marine air temperature since the late nineteenth century. Journal of Geophysical Research: Atmospheres, 108(D14): 4407, doi: 10.1029/2002JD002670

Schmidt G A, Shindell D T, Tsigaridis K. 2014. Reconciling warming trends. Nature Geoscience, 7(3): 158–160, doi: 10.1038/ngeo2105

Shi Rui, Guo Xinyu, Wang Dongxiao, et al. 2015. Seasonal variability in coastal fronts and its influence on sea surface wind in the northern South China Sea. Deep Sea Research Part II: Topical Studies in Oceanography, 119: 30–39, doi: 10.1016/j.dsr2.2013.12.018

Smith S D. 1988. Coefficients for sea surface wind stress, heat flux, and wind profiles as a function of wind speed and temperature. Journal of Geophysical Research: Oceans, 93(C12): 15467–15472, doi: 10.1029/JC093iC12p15467

Su Jilan. 2004. Overview of the South China Sea circulation and its influence on the coastal physical oceanography outside the Pearl River Estuary. Continental Shelf Research, 24(16): 1745–1760, doi: 10.1016/j.csr.2004.06.005

Thompson B, Tkalich P, Malanotte-Rizzoli P. 2017. Regime shift of the South China Sea SST in the late 1990s. Climate Dynamics, 48(5–6): 1873–1882, doi: 10.1007/s00382-016-3178-4

Thomson R E, Emery W J. 2014. Data Analysis Methods in Physical Oceanography. 3rd ed. Waltham, MA: Elsevier Science, 639–664

Trenberth K E, Jones P D, Ambenje P, et al. 2007. Observations: surface and atmospheric climate change. In: Solomon S, Qin D, Manning M, et al., eds. Climate Change 2007: The Physical Science Basis. Contribution of Working Group I to the Fourth Assessment Report of the Intergovernmental Panel on Climate Change. Cambridge and New York: Cambridge University Press, 235–336

Wang Yuntao, Castelao R M, Yuan Yeping. 2015. Seasonal variability of alongshore winds and sea surface temperature fronts in Eastern Boundary Current Systems. Journal of Geophysical Research: Oceans, 120(3): 2385–2400, doi: 10.1002/2014JC010379

Wang Yuntao, Castelao R M. 2016. Variability in the coupling between sea surface temperature and wind stress in the global coastal ocean. Continental Shelf Research, 125: 88–96, doi: 10.1016/j.csr.2016.07.011

Wang Dongxiao, Xie Qiang, Du Yan, et al. 2002. The 1997–1998 warm event in the South China Sea. Chinese Science Bulletin, 47(14): 1221–1227

Wang Zhaoyun, Zhai Fangguo, Li Peiliang. 2016. A shift in the upper-ocean temperature trends in the South China Sea since the late 1990s. Acta Oceanologica Sinica, 35(11): 44–51, doi: 10.1007/s13131-016-0947-1

Wyrtki K. 1961. Physical oceanography of the southeast Asian waters. Scientific Results of Marine Investigations of the South China Sea and the Gulf of Thailand, NAGA Rep. 2. Scripps Institution of Oceanography. La Jolla, California: ICAc Press, 1–225

Xie Shangping, Xie Qiang, Wang Dongxiao, et al. 2003. Summer upwelling in the South China Sea and its role in regional climate variations. Journal of Geophysical Research: Oceans, 108(C8): 3261, doi: 10.1029/2003JC001867

Xue Huijie, Chai Fei, Pettigrew N, et al. 2004. Kuroshio intrusion and the circulation in the South China Sea. Journal of Geophysical Research: Oceans, 109(C2): C02017

Yang Haiyuan, Wu Lixin. 2012. Trends of upper-layer circulation in the South China Sea during 1959-2008. Journal of Geophysical Research: Oceans, 117(C8): C08037

Zhang Liping, Wu Lixin, Lin Xiaopei, et al. 2010. Modes and mechanisms of sea surface temperature low-frequency variations over the coastal China seas. Journal of Geophysical Research: Oceans, 115(C8): C08031